Development and validation of a coupled storm surge and wave model for the coast of Shanghai

Xiuji Zhang*, Yunxiao Jin, Huijie Zhu, Huaihui Song, Yanhong Wang

College of Civil Engineering, Luoyang Institute of Science and Technology, Luoyang 471023, China,
email: zhangxiuji1987@163.com (X. Zhang)

ABSTRACT

A two-dimensional storm surge model coupled with Simulating WAves Nearshore mode was proposed. The coupled terms included radiation stress, wave-dependent surface stress and wave-dependent bottom stress. Numerical experiments were designed to analyze the contribution of waves to the storm surge generated by Typhoon Winnie along the coast of Shanghai. The results revealed that the effects of waves were only slightly significant within the shallow estuarine region, contributing 0.19 m to the peak surge height at the four tidal stations averagely. The influence of waves was partly dependent on the topographic and hydrological features, and it was more obvious for the upper Yangtze River. The inclusion of wave-dependent surface wind stress effects with Myrhaug's wind drag formula improved the model results, contributing up to 9.6% to the peak surge rises than Large's wind drag formula.

Keywords: Finite volume method; Wave-induced surge; Typhoon Winnie; Radiation stress; Wind drag; Bottom stress

1. Introduction

Coastal areas are exposed to severe damage and life-threatening risks from storm surges. The ability to predict these events is critical to the early warning and evacuation procedures implemented by disaster management and relief agencies. Accurate prediction of storm surges has a non-negligible impact on the engineering and construction of human societies. The combination of inverse barometric effects and air-sea interactions is the most important contributor to storm surges. Under typhoon conditions, the transfer of momentum from the atmosphere into the ocean results in the generation of the surges and waves which then interact. The generated wave field can affect water levels and currents in the inshore areas through introducing radiation stresses, which generate longshore currents and wave setup. Besides, waves may change the surface roughness's, which affects surge generation, and enhance the bottom roughness's by generating currents in shallow water.

In many established storm surge models, wind-current interaction was fully considered, while wave effects on storm surges were usually neglected, especially under the conditions of complex topography and hydrological features [1,2]. However, with the development of unstructured grid coupling techniques, wave-current coupling effects have been taken into account in storm surge modeling [3]. The magnitude of wave effects on storm surge simulation is dependent on local topographical and hydrological feature. A tightly coupled Simulating WAves Nearshore SWAN + ADCIRC utilized model unstructured-mesh was validated by Hurricanes Katrina and Rita, which demonstrated the importance of inclusion of the wave-current interactions, and considered that waves and circulation processes should be coupled in many coastal applications, because the water levels could be increased by wind-driven waves 5%–20% in the broad continental shelf regions, and 35%–40% in the narrow shelf or steep slopes regions [4]. Some studies conducted in the Gulf of Mexico also indicated

* Corresponding author.

that the influence of waves on storm surges was significant and should not be neglected in storm surge forecast or hindcast [5,6]. The wave-current coupled simulations study on the nearshore area of Korea showed that wave-induced surges contribute most to the peak surge height in nearshore areas [7]. Vatvani et al. [8] noted that the wind drag parameter was important in the study of wave effects on storm surges. Selection of the appropriate theoretical wind field model was a significant consideration for surge and wave modeling [9]. However, few researches have considered wave effects on storm surges along the coastal areas of Shanghai. Shanghai, located at the northwest edge of the world's largest tropical storm basin (Northwest Pacific Storm Basin), the center point of the north and south coasts of China, and the confluence of the Yangtze River and the Huangpu River into the sea, has intricate relatively shallow topographical feature and complicated hydrological characteristics. The coast of Shanghai is often intruded by storm surges induced by typhoons, including the unfavourable combination with high astronomical tides and upstream flood, resulting in regional flooding, inundation and extensive loss of life and property.

This paper investigate the effects of wave-current coupling on increases in water levels. The effects of wave-induced forces on the storm surge simulation were taken into account by coupling SWAN wave model to a two-dimensional (2D) typhoon-induced storm surge model (named SWEFVM) based on the unstructured grid finite-volume method. The coupling terms, including radiation stress, wave-dependent surface wind stress and wave-dependent bottom stress, had been extended to account for the current field and surge heights. The coupled model was applied to hindcast the storm surges generated by Typhoon Winnie along the coast of Shanghai. Numerical experiments applying different wind drag formula using SWEFVM model and the coupled model were performed to examine the effects of waves on storm surges and to check the behaviour of wind drag parameterization on computed surge levels.

2. Method

The coupled storm surge and wave model was developed to test the wave-current interaction impact on storm surges for the coast of Shanghai. The component SWAN and SWEFVM models are described, and the tight coupling mechanics is introduced in this section. SWAN and SWEFVM are run on the same unstructured grid.

2.1. SWAN model

SWAN model is a third-generation wave model suitable for forecasting wind, surge and waves in coastal, lake and estuarine waters. The model uses a two-dimensional dynamic spectral density conservation equation to represent the accompanying waves with sources and sinks. The wave spectral action density $N(t, x, y, \sigma, \theta)$ is allowed to evolve in time (t), geographical space (x, y) and spectral space (σ, θ), as governed by the action balance equation expressed for Cartesian coordinates:

$$\frac{\partial N}{\partial t} + \frac{\partial c_x N}{\partial x} + \frac{\partial c_y N}{\partial y} + \frac{\partial c_\sigma N}{\partial \sigma} + \frac{\partial c_\theta N}{\partial \theta} = \frac{S_{\text{tot}}}{\sigma} \tag{1}$$

where $c_x = c_{gx} + U_x$ and $c_y = c_{gy} + U_y$ are the propagation velocities of wave energy in spatial x-, y-spaces (c_g and U are wave group speed and current speed), and c_σ, c_θ are the propagation velocities in spectral σ-, θ- spaces (σ is the relative radian frequency, and θ is the wave propagation direction). The source/sink term S_{tot} represents all physical processes that generate, dissipate, or redistribute wave energy. The last four terms on the left-hand side represent the effects of currents on waves. The second and third terms denote the propagation of wave energy in 2D geographical spaces. The fourth and fifth terms represent the shifting of the relative frequency and wave refraction due to variations in water depths and currents.

This paper used SWAN code version 40.85 that solve the spectral action balance equation without any a priori restrictions on the spectrum for the evolution of wave growth by employing an implicit finite difference method. SWAN computations can be applied on an unstructured grid (only triangular meshes) based on a sweeping Gauss–Seidel technique and accompanied by a locally implicit but globally explicit scheme [10]. The use of unstructured grids allows local mesh refinement in areas of interest and offers a high flexibility to generate grids along coastline and around islands.

2.2. Hydrodynamic model

SWEFVM model based on two-dimensional (2D) shallow-water equations (SWE) was applied to the simulation of tides and storm surges at a range of scales [11]. The conservative form of 2D SWE in the Cartesian coordinates is formulated as:

$$\frac{\partial U}{\partial t} + \frac{\partial F(U)}{\partial x} + \frac{\partial G(U)}{\partial y} = B(U) \tag{2}$$

where $U = (h, hu, hv)^T = (h, q_x, q_y)^T$ denotes the state variable vector (h is the bathymetric depth; and u and v are the depth-averaged velocities in the x and y directions); and $F = (hu, hu^2 + gh^2/2, huv)^T$ and $G = (hv, huv, hv^2 + gh^2/2)^T$ are the flux vectors in the x and y directions (g is the gravitational acceleration). The source term vector B is given by:

$$B = \left[0, gh\left(S_{0x} + \frac{\tau_{sx,\text{wind}} + \tau_{sx,\text{wave}} - \tau_{bx}}{\gamma} - \frac{\partial_x P}{\gamma} \right), gh\left(S_{0y} + \frac{\tau_{sy,\text{wind}} + \tau_{sy,\text{wave}} - \tau_{by}}{\gamma} - \frac{\partial_y P}{\gamma} \right) \right]^T \tag{3}$$

where $\gamma = \rho_g$ (ρ is the density of water); S_{0x} and S_{0y} are the bottom slopes in the x and y directions; $\tau_{sx,\text{wind}} = C_d \rho_a W_x |W|$ and $\tau_{sy,\text{wind}} = C_d \rho_a W_y |W|$ are the surface wind stresses (C_d is the wind drag coefficient, and W_x and W_y are the x-component and y-component of wind speed W, respectively); $\tau_{sx,\text{wave}}$ and $\tau_{sy,\text{wave}}$ are radiation stresses due to waves;

$\tau_{bx} = \rho g n^2 u h^{-1/3} \sqrt{u^2 + v^2}$ and $\tau_{by} = \rho g n^2 u h^{-1/3} \sqrt{u^2 + v^2}$ are bottom stresses (n is the Manning coefficient of roughness); and P is the atmospheric pressure at the sea surface.

The wind drag coefficient is affected by the wind speed [12,13].

$$C_d = 0.001 \frac{\rho_a}{\rho} \left(0.49 + 0.065|W|\right) \tag{4}$$

where ρ_a is the density of air.

Water levels and the depth-averaged currents were obtained through solution of the 2D SWE by adopting the unstructured grid finite volume method (FVM). The stage hydrograph, in the case of a storm, astronomical tide, upstream flood, and so on, could be simulated by given initial and boundary conditions.

The HLLC (Harten, Lax, Leer, Contact) solver with high spatial resolution was implemented to compute the normal mass and momentum fluxes [14]. The temporal discretization was carried out by using the explicit Euler scheme. The CFL (Courant–Friedrichs–Lewy) condition should be met in the model to guarantee the stability of numerical calculations.

To simulate the water covering and uncovering processes in the intertidal zone stably and accurately, a wetting-drying scheme was included in the model. The wetting-drying scheme was employed once per time step by dynamically examining the hydraulic condition of the cell interface and selecting corresponding method to compute interfacial fluxes according to the interface type. A tiny critical water depth ε, which was introduced to determine the status of the considered and adjacent cells, was set as 0.001 m in this model. The water depths on the left and right side of the considered cell, h_L and h_R, are computed. For the cases when $h_L < \varepsilon$ and $h_R < \varepsilon$, the mass and momentum fluxes are zero. For the cases when $h_L < \varepsilon$ or $h_R < \varepsilon$, according to water depths and bed elevations of considered and adjacent cells, the interface type would be considered as solid wall or broad crested weir and the fluxes should be computed differently. For the cases when $h_L > \varepsilon$ and $h_R > \varepsilon$, the normal routine of HLLC solver is used to compute the flexes.

2.3. Coupled storm surge and wave model

SWEFVM and SWAN were tightly coupled and run on the same unstructured triangular grid resulting in a more accurate and efficient solution technique. The coupling procedure is illustrated in Fig. 1.

The wind-pressure fields of typhoons generated by the Fujita's model [15], a widely used analytical cyclone model, were inputted to SWEFVM serving as driving forces and accounting for surface roughness. These input wind parameters are interpolated spatially and temporally and projected to the computational grid cells in SWEFVM. The water levels and currents are computed and stored at the center of grid cells in SWEFVM before being passed to SWAN with the wind parameters. These variables are projected to the nodes taking the area-weighted averages of variables on cells adjacent to each node in SWEFVM, and then passed to SWAN, where they are used to calculate relevant wave processes.

SWEFVM is driven partly by wave radiation stresses, wave-dependent surface wind stresses and wave-dependent bottom stresses that are computed using information from SWAN. The wave radiation stresses [16] computed by SWAN is given by:

$$\tau_{sx,\text{wave}} = -\frac{\partial S_{xx}}{\partial x} - \frac{\partial S_{xy}}{\partial x}$$
$$\tau_{sy,\text{wave}} = -\frac{\partial S_{xy}}{\partial x} - \frac{\partial S_{xy}}{\partial x} \tag{5}$$

The gradients of the radiation stresses S_{xx}, S_{xy} and S_{yy} are defined as:

$$S_{xx} = \rho g \int \left[n\cos^2\theta + n - 0.5 \right] \sigma N(\sigma,\theta) d\sigma d\theta$$
$$S_{xy} = S_{yx} = \rho g \int n\sin\theta\cos\theta \sigma N(\sigma,\theta) d\sigma d\theta \tag{6}$$
$$S_{yy} = \rho g \int \left[n\sin^2\theta + n - 0.5 \right] \sigma N(\sigma,\theta) d\sigma d\theta$$

where n is the ratio of group velocity and phase velocity.

In this study, the Donelan formula [17] was employed to evaluate surface roughness length z_0 by considering wave effects.

$$z_0 = 0.000037 \frac{U_{10}^2}{g} \left(\frac{c_P}{U_{10}} \right)^{-0.9} = 0.000037 \frac{U_{10}^2}{g} \left(\frac{g}{2\pi} \frac{T_P}{U_{10}} \right)^{-0.9} \tag{7}$$

where U_{10} is the mean wind speed at the elevation 10 m above sea surface; c_p is the phase speed associated with wind waves with peak frequency. The wave-dependent wind drag coefficient [18] is calculated by:

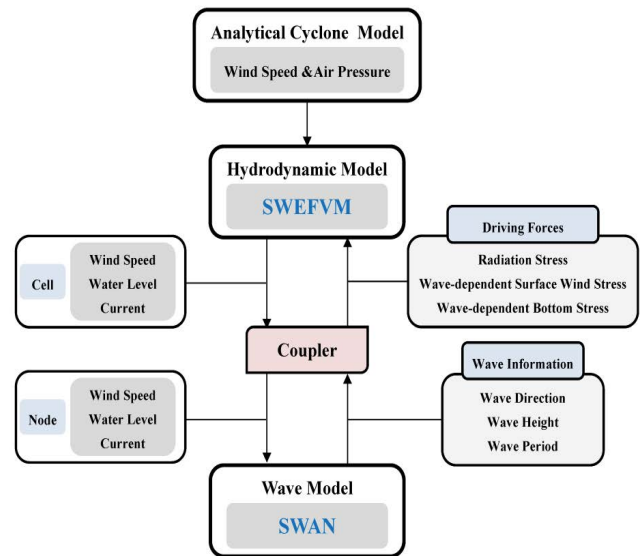$$C_d = \kappa^2 \left(\ln\left(\frac{10}{z_0} \right) \right)^{-2} \tag{8}$$

Fig. 1. Schematic diagram for the coupled model.

where κ is the Karman constant (κ = 0.4).

The wave-dependent bottom stresses [19] are computed by:

$$\tau_{bx} = \rho C_f u \sqrt{u^2 + v^2}$$
$$\tau_{by} = \rho C_f v \sqrt{u^2 + v^2} \tag{9}$$
$$C_f = 2\left[\frac{\kappa}{\ln(h/k_w) - 1}\right]^2$$

where C_f is the bottom friction coefficient, and the apparent bed (wave) roughness k_w is obtained by:

$$\frac{k_w}{k_d} = \frac{h}{k_d}\tanh\left(\frac{k_d}{h}10^f\right)\left(70° \le \Phi \le 90°\right)$$
$$\frac{k_w}{k_d} = \frac{h}{k_d}\tanh\left(\frac{k_d}{h}10^{f+G_f(1.22-\Phi)}\right)\left(0° \le \Phi \le 70°\right) \tag{10}$$

where k_d is the bed roughness; f is the fitting function; G_f is the approximation of slope coefficient; and Φ is the angle between wave and current.

The values of wave radiation stresses, wave-dependent surface wind stresses and wave-dependent bottom stresses inside each cell used in SWEFVM are simply the average of these stresses in the associated nodes of the cell computed by SWAN.

The time step of SWEFVM is relatively small comparing to that of SWAN, whose time step can be relatively large due to its unconditional stable property. The present hindcasts utilized SWAN time step of 600 s, and SWEFVM time step was 5 s. The coupling interval was taken to be the same as the SWAN time step. The two models run sequentially, so that either SWAN or SWEFVM is alternatively running.

SWEFVM runs first on the coupling interval, using wave radiation stresses, wave-dependent surface wind stresses and wave-dependent bottom stresses from SWAN during the interval to interpolate its wave forcing in time. After its last time step in the coupling interval, SWEFVM passes wind velocities, water levels, and currents to SWAN. Then SWAN runs on the next interval, using the variables from the computations of SWEFVM in the interval. After its time step, SWAN computes the wave radiation stresses, wave-dependent surface wind stresses and wave-dependent bottom stresses, and passes them to SWEFVM, which then begins a new process in the next interval.

2.3. Model grids and boundary conditions

The accuracy of simulated storm surges significantly depends on the use of a suitably large physical domain. The coupled storm surge and wave model was applied to the coastal area of Shanghai, covering the small-scale Huangpu River, the medium-scale Yangtze River estuary and Hangzhou Bay, and the large-scale part of the East China Sea. The computational domain is bounded by the Yangtze River in the north, the East China Sea in the east, Hangzhou Bay in the south, and covers a range of 120.9–123.6°E in

longitude and 29.5–33°N in latitude. The wide range of cell sizes demonstrates the significant advantages of an unstructured grid: resolution is governed by local flow scales. The unstructured grids (Fig. 2) used in this work contains 3162 nodes and 5634 triangular cells. Grid resolution varies from approxmately 8 km in the open sea, to hundreds of meters on the continental shelf such as the shallow areas of the Yangtze estuary, to less than 100 m in the Huangpu River.

The normal flow at the wall boundary (closed boundary) is set to be zero. Besides, the coupled model consists of two freshwater inflow boundaries (Yangtze estuary and Huangpu River boundaries), Hangzhou Bay open boundary and the open sea boundary (Fig. 2). For the inflow boundaries of Huangpu River and Yangtze estuary, the measured water levels from Mishidu and Xuliujing stations are used respectively; for the open boundary of Hangzhou Bay, the measured data from Zhapu station are used. In tide simulations, eight major tidal components (K_1, O_1, P_1, Q_1, M_2, S_2, N_2 and K_2) obtained from a global tide model [20] are used as harmonics constants and applied to open sea boundary points.

2.4. Simulation conditions

This paper focused on investigating the influence of wave-current coupled procedure between hydrodynamic and wave models on storm surge heights. Three scenarios were simulated:

- Case 1: Simulation using SWEFVM model with Large's wind drag formula (model-run UL: uncoupled – Large's c_d);
- Case 2: Simulation using the coupled model with Large's wind drag formula (model-run CL: coupled – Large's c_d);
- Case 3: Simulation using the coupled model with Myrhaug's wind drag formula (model-run CM: coupled – Myrhaug's c_d).
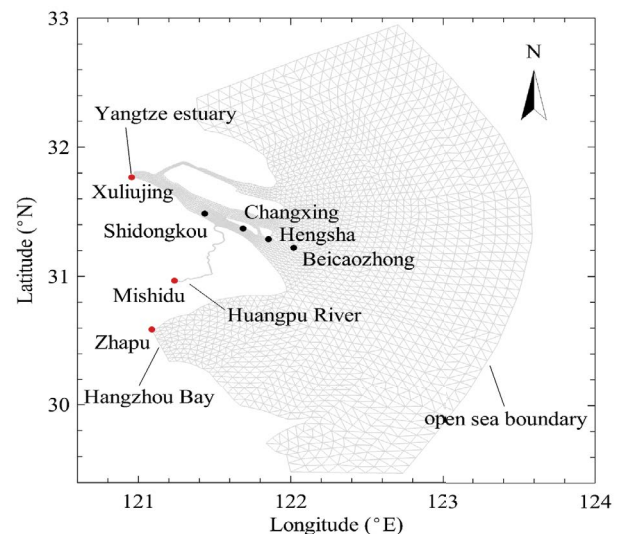

Fig. 2. Unstructured grids for the computational domain and locations of tidal stations and open boundaries.

3. Results

The base run, CM, investigated the results of storm surge and wave simulation during Typhoon Winnie (Fig. 3). The UL and CM model scenarios were run to examine the impact of wave-current coupling on computed surge levels. The CL and CM model scenarios were designed to reveal the behaviour of different wind drag formulas on storm surge results.

The input data of typhoon track, pressure at typhoon centre and maximum wind speed for Typhoon Winnie was obtained from the China Meteorological Administration (CMA) Tropical Cyclone Best Track Dataset.
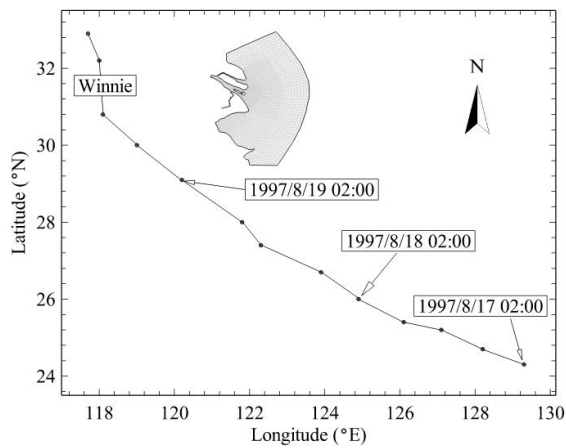

Fig. 3. Track of Typhoon Winnie.

3.1. Model validations

The coupled storm surge and wave model was validated through its application to hindcast of Typhoon Winnie. For comparison with observations, the time series of computed water levels were stored and compared at a number of tidal stations. In this paper, the results at four representative tidal stations along the Yangtze River estuary, that is, Shidongkou, Changxing, Hengsha and Beicaozhong, were presented. Shidongkou station is located at the upper reaches of the Yangtze River estuary, and Beicaozhong station is located at the confluence of the Yangtze River and the East China Sea. An overview of the station locations was given in Fig. 2.

During the 48-h simulation, four high water levels occurred at each station. The hydrograph and phase of the water levels simulated by model run CM (model run that did consider the effect of waves and wave-current interaction) were in good agreement with observations (Fig. 4). The root mean square errors (RMSE) in water level at different gauges range from 0.46 to 0.56 m, Many of the better applied models have an RMSE range from 0.28 to 1.26 m [21]. Although the model results sometimes underestimated or overestimated the water level, the results were sufficient to represent the reasonable accuracy of storm surge simulation.

3.2. Effects of wave-current interaction on storm surges

To investigate the effects of wave-current interaction on the model results, the wave-induced surge was evaluated by subtracting the results of the UL run (model run
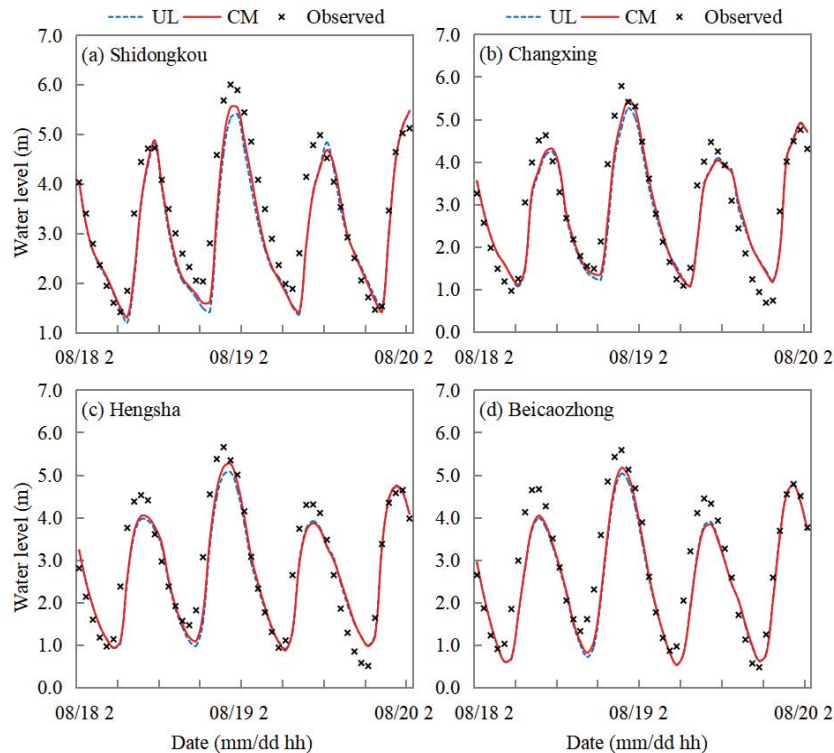

Fig. 4. Comparison of simulated water levels using model runs UL and CM with observations at tidal stations for Typhoon Winnie.

without considering the waves) from the results of the CM run. The time series of the contribution of the wave-induced surge are depicted in Fig. 5. The contribution of waves to surge heights was mainly increase, especially at the peak water levels. And this wave set-up effect was highest at Shidongkou station, and gradually decreased along the Yangtze River to Beicaozhong station.

The statistical errors for the differences between the simulated and observed water levels of model runs UL and CM at four tidal stations could be found in Table 1. The RMSE was reduced from 0.50–0.60 m to 0.46–0.56 m, taking into account the effects of waves. And the mean absolute error (MAE) was also reduced. The simulated results were improved more significantly at Shidongkou station, and the improvement was less effective at Beicaozhong station. The comparison of the Peak water levels showed that although the simulation results of both model runs underestimated the water levels, the full coupled model run CM improved the simulation results for all stations, including an improvement of 0.21 m at Shidongkou station, 0.20 m at Changxing and Hengsha stations, and 0.13 m at Beicaozhong station. The results of the model run CM, considering the effects of wave-current interaction, agreed better with the observed values than those of the model run UL.

3.3. Effects of the wind drag parameterisation on storm surges

To compare the effects of two different wind drag formulas on the storm surge simulation, the astronomical tide was removed from the total water level to obtain the storm surge height. The computed surge heights for model runs CL (applying Large's wind drag formula) and CM (applying Myrhaug's wind drag formula) were compared to the observed surge heights at the four tidal stations in Fig. 6.
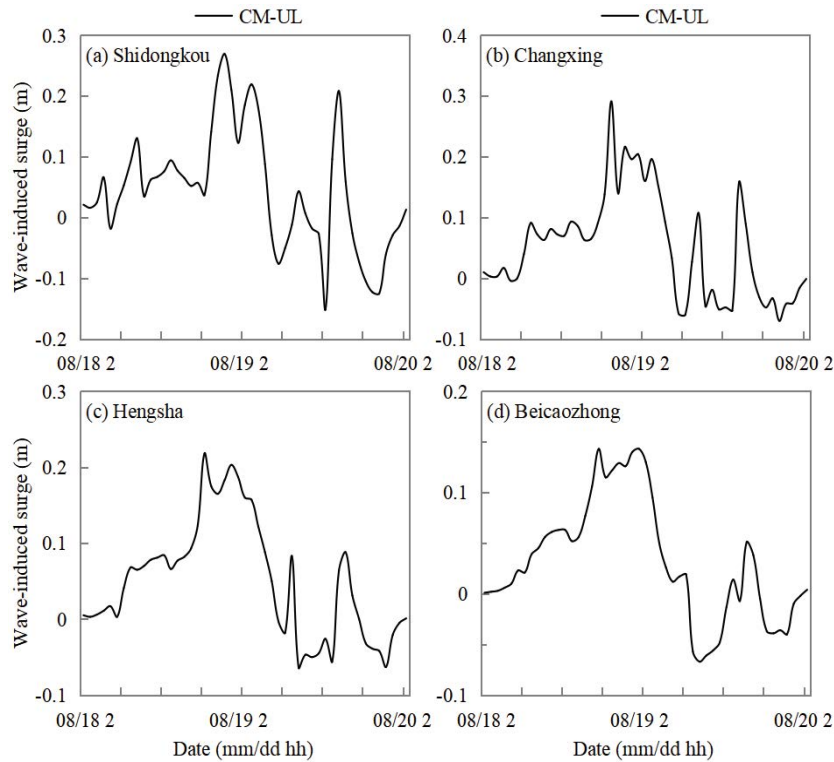

Fig. 5. Wave-induced surge heights evaluated by subtracting the results of the UL run from those of the CM run at tidal stations for Typhoon Winnie.

Table 1
Statistical errors and comparison of peak water levels at tidal stations for model runs UL and CM

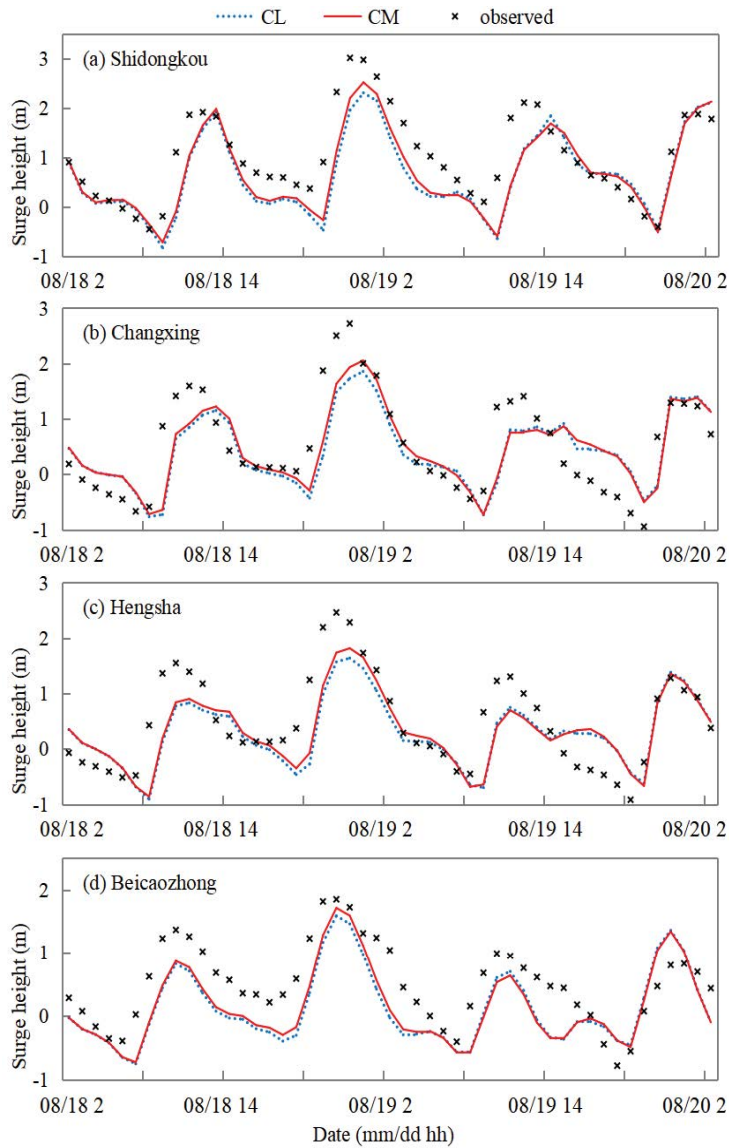| Station	UL-water level (m)		CM-water level (m)		Peak water level (m)		
	MAE	RMSE	MAE	RMSE	Observation	CL	CM
Shidongkou	0.48	0.50	0.43	0.46	6.00	5.33	5.54
Changxing	0.45	0.60	0.42	0.56	5.78	5.26	5.46
Hengsha	0.44	0.56	0.42	0.53	5.65	5.06	5.26
Beicaozhong	0.50	0.53	0.48	0.52	5.58	5.03	5.16

Fig. 6. Comparison of simulated surge heights using model runs CL and CM with observations at tidal stations for Typhoon Winnie.

During the peak water level moment, the differences between the simulated surge heights of model runs CL and CM at the four tidal stations were 0.12–0.21 m (Table 2), while the differences were less significant at other moments. The Maximum improvement of simulated peak surge height by model run CM was 11.0% for Hengsha station, while the minimum improvement was 7.5% for Beicaozhong station. The simulation results of model run CM, considering the effect of wave-dependent surface wind stresses on storm surges using Myrhaug's wind drag formula, fit better with the observed values than those of the model run CL.

4. Discussion

The validation results of Model run CM indicated that this full coupled model developed for the coast of Shanghai could effectively simulate the typhoon-induced storm

Table 2
Comparisons of peak surge heights at tidal stations for model runs CL and CM

Station	Peak surge height			
	Observation (m)	CL (m)	CM (m)	Improvement (%)
Shidongkou	3.02	2.31	2.52	9.1
Changxing	2.72	1.85	2.05	10.8
Hengsha	2.46	1.64	1.82	11.0
Beicaozhong	1.85	1.59	1.71	7.5

surge with an average relative error of only 6.91% at the peak water levels (Table 1). However the simulated water levels were sometimes underestimated or overestimated.

These discrepancies may be due to the inaccuracy of the wind field and air pressure field, which was created by the parametric cyclone model that had difficulty reproducing different wind conditions of those locations far away from the typhoon center.

When the wave effects were included, the simulation results of model run CM were more consistent with the observed results than those of model run UL, and the average improvement of the simulated peak water level was 0.19 m. It was due to take into account wave radiation stress, wave-dependent surface wind stress and wave-dependent bottom stress that induced by waves comprehensively. The MAE and RMAE of the simulated water levels was reduced by considering wave effects, and the improvement was more significant at Shidongkou station, which is located at the upstream of the Yangtze estuary, while the improvement is relatively low at Beicaozhong station, which is near the open coast. It was indicated that this full coupled storm surge and wave model was applicable to the coast of Shanghai. The wave-induced contribution to the surge heights at the mouth of the Yangtze River was not as strong as that suggested by Dietrich et al., on account of the gentle longitudinal slope of the river bottom.

The observed surge heights of Shidongkou and Changxing stations, which were located in the upper reaches of the Yangtze River, were larger than the other stations, due to the narrower channel, and the peak storm surge heights were more than 3 m. The simulation results of model run CM agreed better to the observed values than those of model run CL, although the simulated peak surge heights of both underestimated the surge heights at the four stations. The minimum error of simulated peak surge heights by model run CM was 0.14 m for Beicaozhong station, while the errors of the other three stations were 0.50–0.67 m. On the contrary, the simulation considering the wave effects at the other three stations showed improvement of 9.1%–11.0%, higher than 7.5% at Beicaozhong station. It may be owed to the fact that Beicaozhong station was located in a wide water area and less influenced by the topography and wave set-up. In general, the comparison results of model runs CL and CM showed that the set-up generated by wave was more sensitive to the application of Myrhaug's wind drag formula.

5. Conclusion

Wave-current interaction is important in determining the nearshore current profile and the total water levels. A 2D storm surge (SWEFVM, based on the unstructured grid finite-volume method) and wave (SWAN) coupled model was developed and applied to simulate the storm surges along the coast of Shanghai. Coupling between waves and currents was achieved in three ways: (1) radiation stress; (2) wave-dependent surface wind stress; (3) wave-dependent bottom stress. The coupled model had been assessed using a storm event induced by Typhoon Winnie along the coast of Shanghai. The model validation results showed that the simulated water levels agreed well with the observed values in both magnitude and phase. The wave-induced surge could reach to 0.21 m at Shidongkou station, slightly higher

in the narrow upper reaches of the Yangtze River than at the mouth of the Yangtze River. Applying Myrhaug's wind drag formula for wave-dependent surface wind stress produced clearly improved results in storm surge simulation, contributing up to 9.6% to the peak surge rises. Besides, the simulation accuracy was also affected by the topography and other factors. Hence, these results implied that the coupled model is suitable for application in storm surge simulation along the coast of Shanghai and similar regions, and the effect of waves and choice of Myrhaug's wind drag formula should be taken into account when determining storm surge heights.

References

[1] M.I. Vousdoukas, E. Voukouvalas, A. Annunziato, A. Giardino, L. Feyen, Projections of extreme storm surge levels along Europe, Clim. Dyn., 47 (2016) 1–20.

[2] Y.N. Cheng, S. Tuhaijan, M. Fattah, V.J. Kurian, Z. Mustaffa, Experimental investigation of directional hydrodynamic coefficients and the effects on wave force due to spreading angles, Ain Shams Eng. J., 11 (2020) 1021–1034.

[3] D.M. Xie, Q.P. Zou, J.W. Cannon, Application of SWAN + ADCIRC to tide-surge and wave simulation in Gulf of Maine during Patriot's Day storm, Water Sci. Eng., 9 (2016) 33–41.

[4] W.B. Chen, L.Y. Lin, J. Jiun-Huei, C.H. Chang, Simulation of typhoon-induced storm tides and wind waves for the northeastern coast of Taiwan using a tide–surge–wave coupled model, Water, 9 (2017) 549, doi: 10.3390/w9070549.

[5] D.S. Dukhovskoy, S.L. Morey, Simulation of the hurricane Dennis storm surge and considerations for vertical resolution, Nat. Hazards, 58 (2011) 511–540.

[6] Y. Sun, C. Chen, R.C. Beardsley, Q. Xu, J. Qi, H. Lin, Impact of current-wave interaction on storm surge simulation: a case study for hurricane bob, J. Geophys. Res.: Oceans, 118 (2013) 2685–2701.

[7] J.J. Yoon, K.C. Jun, Coupled storm surge and wave simulations for the southern coast of Korea, Ocean Sci. J., 50 (2015) 9–28.

[8] D. Vatvani, N.C. Zweers, O.M. Van, A.J. Smale, D.H. Vries, V.K. Makin, Storm surge and wave simulations in the Gulf of Mexico using a consistent drag relation for atmospheric and storm surge models, Nat. Hazards Earth Syst. Sci., 12 (2012) 2399–2410.

[9] L.A. Bastidas, J. Knighton, S.W. Kline, Parameter sensitivity and uncertainty analysis for a storm surge and wave model, Nat. Hazards Earth Syst. Sci., 16 (2015) 2195–2210.

[10] M. Zijlema, Computation of wind-wave spectra in coastal waters with SWAN on unstructured grids, Coastal Eng., 57 (2010) 267–277.

[11] X.J. Zhang, D.G. Wang, X.J. Lai, H.H. Song, Effect of forecasted typhoon track uncertainties on storm surge predictions for the coast of Shanghai, J. Hydraul. Res., 54 (2016) 41–55.

[12] W.G. Large, S. Pond, Open ocean momentum flux measurements in moderate to strong winds, J. Phys. Oceanogr., 11 (1981) 324–336.

[13] A.M. Elmoustafa, N.Y. Saad, E.M. Fattouh, Defining the degree of flood hazard using a hydrodynamic approach, a case study: wind turbines field at west of Suez Gulf, Ain Shams Eng. J., 11 (2020) 741–749.

[14] E.F. Toro, M. Spruce, W. Speares, Restoration of the contact surface in the HLL-Riemann solver, Shock Waves, 4 (1994) 25–34.

[15] T. Fujita, Pressure distribution within a typhoon, Geophys. Mag., 23 (1952) 437–451.

[16] M.S. Longuet-Higgins, R.W. Stewart, Radiation stresses in water waves; a physical discussion, with applications, Deep Sea Res. Oceanogr. Abstr., 11 (1964) 529–562.

[17] M.A. Donelan, F.W. Dobson, S.D. Smith, R.J. Anderson, On the dependence of sea surface roughness on wave development, J. Phys. Oceanogr., 23 (1993) 2143–2149.

[18] D. Myrhaug, O.H. Slaattelid, Effects of sea roughness and atmospheric stability on wind wave growth, Ocean Eng., 29 (2002) 1133–1143.

[19] A. Perlin, E. Kit, Apparent roughness in wave-current flow: implication for coastal studies, J. Hydraul. Eng., 130 (2002) 729–741.

[20] G.D. Egbert, S.Y. Erofeeva, Efficient inverse modeling of barotropic ocean tides, J. Atmos. Oceanic Technol., 19 (2002) 183–204.

[21] N. Mamnun, L.M. Bricheno, Md Rashed-Un-Nabi, Forcing ocean model with atmospheric model outputs to simulate storm surge in the Bangladesh coast, Trop. Cyclone Res. Rev., 9 (2020) 46–63.